Int J Adv Manuf Technol (2015) 78:1171–1179
DOI 10.1007/s00170-014-6715-5

ORIGINAL ARTICLE

Modeling machining of particle-reinforced aluminum-based metal matrix composites using cohesive zone elements

U. Umer · M. Ashfaq · J. A. Qudeiri · H. M. A. Hussein · S. N. Danish · A. R. Al-Ahmari

Received: 18 September 2014 / Accepted: 12 December 2014 / Published online: 7 January 2015

Abstract Finite element modeling for the machining of heterogeneous materials like particle-reinforced metal matrix composites has not been much successful as compared to homogeneous metals due to several issues. The most challenging issue is to deal with severe mesh distortion due to nonuniform deformation inside the workpiece. Other problems are related to the modeling of the interface between reinforcement particles and matrix and tool-reinforcement particle interaction. In this study, different strategies are adopted for finite element models (FEM) to cope with the above issues and comparative analyses have been performed. These 2D FE models are based on plane strain formulations and utilize a coupled temperature displacement method. The workpiece is modeled using reinforcement particle size and volume fraction inside the base matrix. The interface between the reinforcement particles and the matrix is modeled by using two approaches, with and without cohesive zone elements, and the chip separation is modeled with and without using a parting line. This allows models to simulate the local effects such as tool-reinforcement particle interaction and reinforcement particle debonding. In addition, the models can predict cutting forces, chip morphology, stresses, and temperature distributions. The effects of different methodologies on the model development, simulation runs, and predicted results have been discussed. The results are compared with experimental data, and it has been found that the utilization of cohesive zone elements (CZE) with the parting line approach seems to be the best one for the modeling of metal matrix composite (MMC) machining.

Keywords Finite element models (FEM) · Metal matrix composites (MMCs) · Cohesive zone elements (CZE)

U. Umer (✉) · M. Ashfaq · J. A. Qudeiri · A. R. Al-Ahmari
FARCAMT, Advanced Manufacturing Institute, King Saud University, Riyadh, Saudi Arabia
e-mail: usamaumer@yahoo.com

H. M. A. Hussein
Advanced Manufacturing Institute, King Saud University, Riyadh, Saudi Arabia

H. M. A. Hussein
Department of Mechanical Engineering, Helwan University, Cairo 11792, Egypt

S. N. Danish
Sustainable Energy Technologies Center, King Saud University, Riyadh, Saudi Arabia

1 Introduction

Metal matrix composites (MMCs), like all composites, consist of at least two chemically and physically distinct phases, suitably distributed to provide properties not obtainable with either of the individual phases. Generally, there are two phases, e.g., a fibrous or particulate phase, distributed in a metallic matrix. MMCs are gradually replacing conventional metals in many engineering applications due to their superior properties like fracture resistance, higher stiffness, and extremely good strength to weight ratio. MMCs are being used in transmission lines, aerospace and automobile parts, and various cutting tools specially oil drilling inserts. Some special physical properties make them an attractive choice for superconducting magnets and thermal management applications [1, 2].

MMCs can be subdivided into three broad categories: (a) equi-axes particle reinforced, (b) short fiber reinforced which may be aligned or not, and (c) long fiber reinforced. The development of a particular MMC for some specific applications depends on the methods of synthesis and fabrication for

stock items. These issues are of particular interest to material technologists and product development engineers [3].

The key issues in the processing of MMCs are the various problems associated with machining, i.e., MMCs have poor machinability as compared to conventional metals. This is mainly due to nonhomogeneity and abrasive nature of reinforcement particles. Mostly, MMCs are fabricated with near net shape processes, but some machining and finishing cuts are indispensable for final dimensions and surface finishes. Cutting tools such as high-speed steel, cast cobalt alloys, cemented carbides, and cermets cannot be used for machining of MMCs due to high wear rate. Diamond cutting tools are found to be the best option for machining of MMCs, and they are being utilized in the last 10 years for both particle- and fiber-based MMCs [4–6].

Fiber-reinforced composites are anisotropic as fibers are not equi-axes, whereas particulate-reinforced composites are isotropic like conventional metals. The latter provide higher ductility and their isotropic nature makes them a better alternative to conventional metals and alloys. The machinability of particulate-reinforced composites depends on many factors like particulate type, its orientation, tool material, tool geometry, and cutting conditions like cutting speed, feed, etc.

Numerous studies exist in the literature to analyze machining of MMCs using experiments and mostly related to measure performance variables like tool wear, surface roughness, subsurface damage, cutting forces, cutting temperatures, and chip morphology [2]. It has been found that parameters related to the structure of composites greatly affect the machinability. These include reinforcement material, reinforcement type, volume fraction of the particles, base metal properties, and overall arrangement of constituent phases. Polycrystalline diamond inserts (PCD) are commonly employed for their machining [7, 8]. The use of other ceramic materials like cubic boron nitride (CBN), alumina, and silicon nitride is also reported but did not have a major success. The effects of cutting parameters (speed, feed, and depth of cut) on machinability of MMCs are almost similar to those found in machining of conventional metals with some differences due to the abrasive nature of particles. A built-up edge is formed while machining these composites at low cutting speeds [9, 10]. This built-up edge increases the rake angle and consequently reduces the cutting forces compared to high cutting speeds. However, some studies have shown a decrease in cutting forces with an increase in cutting speed. Manna and Bhattacharayya machined aluminum-based MMCs reinforced with silicon carbide particles (Al/SiC) using an uncoated carbide tool. They showed that cutting and feed forces decrease with an increase in cutting speed [11]. The reinforced particles tend to expel out from the base metal and slide in front of the cutting tool edge. This results in plowing through the newly generated machined surface and groove marks on it [9, 12].

A lot of research has been done to model orthogonal machining of MMCs using finite element (FE) methods. Researchers used three approaches: (a) micromechanics-based approach, (b) equivalent homogeneous material (EHM) approach, and (c) hybrid approach, i.e., the combination of two [2]. The first two approaches have both advantages and disadvantages [13]. Debonding of reinforced particle and deformation mechanism can be best modeled by the micromechanics approach. However, the approach is computationally very expensive as a very fine mesh is required in contrast to conventional modeling. The EHM approach is unable to predict local effects such as damage at the particle-matrix interface [14, 15], but it reduces simulation time and can predict some performance variables like cutting forces and temperature with a reasonable degree of accuracy. The advantages of both approaches can be obtained using a hybrid approach. A combination of the micromechanical and EHM models is developed by Rao et al. [16] to study orthogonal cutting. The effects of fiber orientation on the cutting forces, chip formation, and fiber damage were analyzed using this approach. The EHM was used to model the overall phenomenon, while the micromechanical model was used near the tool tip and tool-chip interface.

Machining of particulate-reinforced metal matrix composites (PRMMC) has been modeled by various researchers. Except for a few, most of the studies are limited to 2D modeling and plane strain formulation, which can be utilized only for orthogonal machining. On the other hand, 3D modeling requires 3D stress formulation which is computationally expensive as compared to plane strain formulation. In addition, 3D models are complex due to consideration of different tool inclinations and movement of chip in three dimensions. Monaghan and Brazil [17] utilized a 2D finite element code FORGE2 to model failure at the particle-matrix interface and the residual stresses while machining aluminum-based MMCs. However, the interface modeling between particles and matrix was not mentioned and failure was predicted based on stress distribution. A similar study was done by Ramesh et al. [18] to predict cutting forces, stress distribution, and particle debonding. Stress distributions and cutting force requirement were predicted for different tool positions with respect to reinforcement particles. El-Gallab and Sklad [19] developed a model for the machining of SiC-reinforced aluminum alloy. It was found that feed has the largest effect on the subsurface damage and the residual stresses. Both subsurface damage and residual stresses increase with increased feed rate. The study was limited to orthogonal machining and the particles were assumed to be perfectly bonded. Other researchers model the tool-reinforcement particle interaction by considering particles on, above, and below the tool path [3, 20]. Zhou et al. [21] utilized a model for modeling of machining Al/SiC MMCs with a PCD tool. First, a 2D EHM model was developed to predict stress distributions,

Table 1 Different studies for the modeling of machining of MMCs

S. No.	Study	MMC type	Model type	Method	Interface modeling	Output variables	Remarks
1	Monaghan and Brazil [17]	PRMMC	2D	Hybrid	No	Matrix flow, tool wear, and residual stresses	
2	El-Gallab and Sklad [19]	PRMMC	2D	Micromechanics	No	Subsurface damage and residual stresses	
3	Zhu Y and Kishawy HA [3]	PRMMC	2D	Micromechanics	No	Temperature and stress distribution	
4	Pramanik et al. [20]	PRMMC	2D	Micromechanics	Yes	Stress distribution and particle debonding	Modeling debonding by matrix element failure
5	Ramesh et al. [18]	PRMMC	2D	Micromechanics	No	Cutting forces and stress distribution	
6	Zhou et al. [21]	PRMMC	2D	Hybrid	Yes	Cutting forces and stress distribution, and tool-particle interaction	Modeling debonding by matrix element failure
7	Dandekar and Shin [22]	PRMMC	2D/3D	Hybrid	Yes	Cutting forces, stress distribution, and subsurface damage	Modeling debonding by cohesive zone elements
8	Dandekar and Shin [23]	FRMMC	2D	Micromechanics	Yes	Stress distribution, fiber damage, and debonding	Modeling debonding by cohesive zone elements

and then later, it is applied to a micromechanics model to simulate particle debonding. A similar approach was utilized by Dandekar and Shin [22] to model subsurface damage in Al/SiC MMCs. However, the latter model utilized cohesive zone elements (CZE) to simulate debonding of reinforced particles. The authors had also implemented CZE to model fiber fracture and debonding in fiber-reinforced metal matrix composites (FRMMC) [23].

In addition to finite element methods, some researchers utilized particle methods or mesh-free methods for the modeling of machining of composites. The most common are discrete element methods (DEM) and smoothed particle hydrodynamics (SPH). The major advantage of these methods is the elimination of mesh distortion problems and mesh refinement methods. Although DEM are developed for granular or powder-based materials, Iordanoff et al. [24] showed that DEM can also be implemented successfully for the modeling of various metal forming and machining processes. In DEM, the workpiece is supposed to consist of a set of discrete particles that move under a force field. Particles kinematics are obtained by using an explicit algorithm to integrate the dynamic Newton's law. This methodology had been implemented by Iliescu et al. [25] to model orthogonal cutting of a unidirectional carbon fiber-reinforced polymer. Cutting forces and fiber debonding had been simulated and found to be in good agreement with the experimental results. In comparison to DEM, SPH methods are more commonly employed in modeling of machining processes as they are developed for continuum materials like FEM. However, except for a few [26, 27], most of the studies are limited to homogeneous materials and are unable to perform coupled temperature-displacement analysis. In addition, the relationships between many SPH parameters (e.g., numerical formulation and particle spacing) with chip morphology are still unknown and need

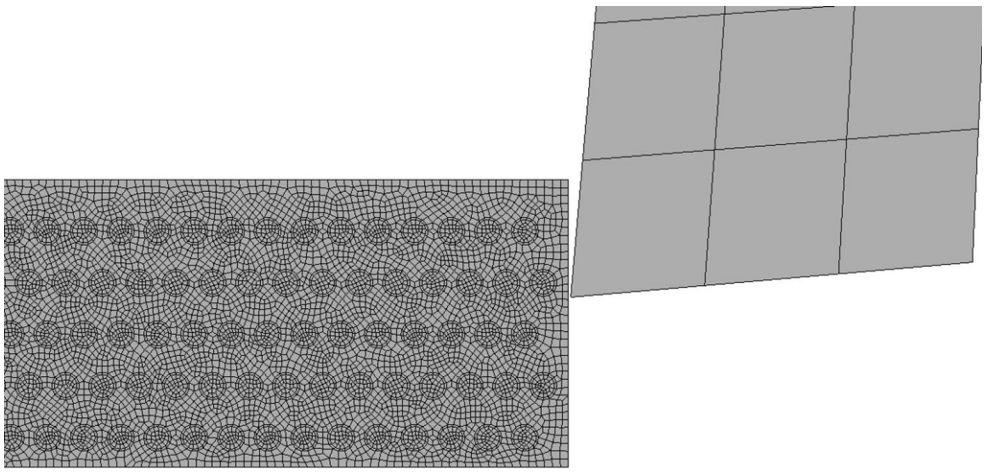

Fig. 1 FE model without parting line

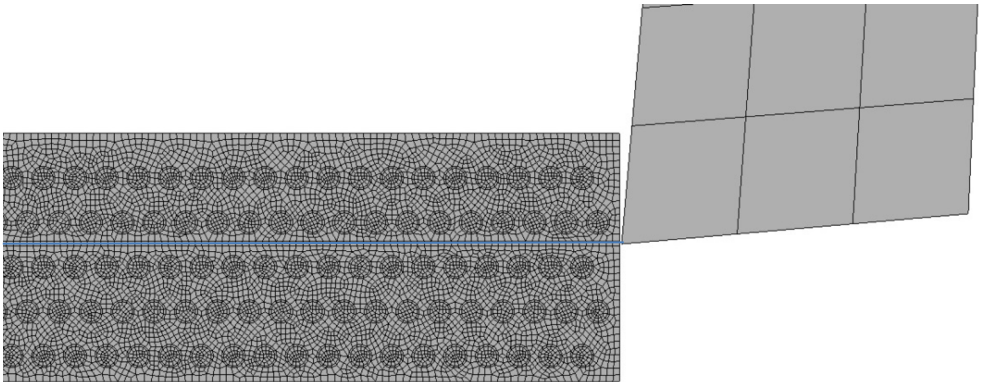

Fig. 2 FE model with parting line

further investigations [28]. Table 1 highlights different modeling studies done in the past 20 years for machining of MMCs.

The aim of the present study is to investigate different methodologies to model orthogonal machining of SiC particle-reinforced aluminum-based metal matrix composites using PCD tools. The reinforced particle average size is around 20 μm and the volume fraction is 20 %. A heterogeneous workpiece model based on reinforcement particle size and volume fraction is used to simulate the local effects such as particle debonding and tool-particle interactions. The experimental results published in [22] have been used to verify the different FE models.

2 Finite element models

FE models are developed using a general-purpose FE software ABAQUS®. Explicit dynamic analysis with coupled temperature displacement procedure is used for each model. Lagrangian formulation is adopted in which the workpiece is fixed and the tool moves with a constant speed. The chip separation is realized by element deletion method using two approaches, i.e., with and without a parting line. Similarly, the interface between the reinforcement particles and the matrix is modeled by with and without cohesive zone elements. Undeformed meshes for FE models with and without a parting line are shown in Figs. 1 and 2. The workpiece and cutting tool material properties are shown in Table 2, and the cutting parameters are shown in Table 3.

For the aluminum matrix, the Johnson and Cook constitutive model is used to include stress variations due to strain, strain rate, and temperature. This relationship is frequently adopted for dynamic problems with high strain rates and temperature effects.

$$\sigma = (A + B\varepsilon^n)\left(1 + C\ln\left(\frac{\dot{\varepsilon}}{\dot{\varepsilon}_0}\right)\right)\left(1-\left(\frac{T-T_{\text{room}}}{T_{\text{melt}}-T_{\text{room}}}\right)^m\right) \quad (1)$$

where ε is the equivalent plastic strain, $\dot{\varepsilon}$ the equivalent plastic strain rate, and T the operating temperature. The Johnson and Cook equation has five material constants, which are A for yield stress constant, B for strain hardening constant, n for strain hardening exponent, C for strain rate hardening constant, and m for temperature dependency coefficient. T_{room} and T_{melt} are room and melting temperatures and are taken as 20 and 593 °C, respectively. The material constants are determined from experiment results and can include data over a wide range of strain rates and temperatures. Due to the nonlinear dependence of the flow stress of the material during plastic strain, an accurate value of stress requires expensive iteration for calculation of the increment plastic strain. Johnson and Cook parameters utilized in the simulations are shown in Table 4.

Table 2 Composition and properties of workpiece and cutting tool materials

	Workpiece (aluminum matrix A359 alloy)	Reinforcement particles (SiC)	Cutting tool (PCD)
Density (kg/m^3)	2700	4370	3500
Young's modulus (GPa)	72	408	800
Thermal conductivity (W/m/°C)	180	30	173
Specific heat (J/Kg/°C)	963	706	508

Table 3 Cutting parameters and tool geometry for FE model

Cutting parameters	
Speed	300 m/min
Feed rate	0.1 mm/rev
Depth of cut	1 mm
Cutting tool geometry	
Rake angle	5°
Clearance angle	5°
Edge preparation	No

Table 4 The Johnson and Cook flow model's parameters

JC parameters	A (MPa)	B (MPa)	C	n	m
	255	361	0.01	0.18	5.5

The chip separation in the chip is simulated using the Johnson and Cook damage law which takes into account strain, strain rate, temperature, and pressure [29]. The damage was calculated for each element and is defined by

$$D = \sum \frac{\Delta\varepsilon}{\Delta\varepsilon_f} \tag{2}$$

where $\Delta\varepsilon$ is the increment of equivalent plastic strain during an integration step and $\Delta\varepsilon_f$ is the equivalent strain to fracture, under the current conditions. Fracture is then allowed to occur when D=1.0, and the concerned elements are removed from the computation. The general expression for the fracture strain is given by

$$\varepsilon_f = \left(D_1 + D_2\exp\left(D_3\sigma^*\right)\right)\left(1 + D_4\ln\left(\frac{\dot{\varepsilon}}{\dot{\varepsilon}_0}\right)\right)\left(1 - D_5\left(\frac{T - T_{\text{room}}}{T_{\text{melt}} - T_{\text{room}}}\right)^m\right) \tag{3}$$

where $\dot{\varepsilon}_o$ is the reference strain rate and σ^* is the ratio of pressure stress to von Mises stress. D_1 to D_5 are material constants and determined by tensile and torsion tests. The Johnson and Cook damage parameters for AISI H13 are listed in Table 5.

Both the tool and reinforcement materials are modeled as linear elastic without considering fracture.

The contact between the tool and workpiece is modeled using sliding-sticking friction model. The division of the sliding and sticking regions is determined by Eq. 4:

$$\begin{aligned} s &= \mu p \text{ when } \mu p < T_{\max} \\ s &= T_{\max} \text{ when } \mu p \geq T_{\max} \end{aligned} \tag{4}$$

where s, p, and $T_{\max}$ are the friction, normal, and maximum equivalent shear stresses at the tool rake face. The second approach is adopted in this analysis with a (coefficient of friction) value of 0.15 [3].

The interface between the reinforcement particles and the aluminum matrix is modeled by cohesive zone elements. The cohesive zone element (CZE) works by defining a relationship between interfacial force (traction) and crack opening displacement (separation). The fracture zone is assumed to have initially zero thickness and consists of two identical cohesive surfaces. The separation between the two surfaces under a prescribed load is given by a traction-separation law. The stiffness of the cohesive elements degrades as the separation increases, and finally, the elements are deleted upon a specified maximum value. In this study, cohesive element stiffness and traction-separation behavior are implemented based on a study done in [30]. The elastic and shear moduli for cohesive elements are taken to be 180.6 and 76.6 GPa, respectively. The maximum stress for mode I and mode II loading is summarized in Table 6.

Table 5 Parameters for the Johnson and Cook damage law

JC parameters	D_1	D_2	D_3	D_4	D_5
	0.071	1.248	−1.142	0.147	0.1

Table 6 Maximum stress corresponding to traction separation behaviour for cohesive elements

No.	Temperature (°C)	Maximum stress mode I (GPa)	Maximum stress mode II (GPa)
1	23	3.77	2.76
2	200	3.30	2.41
3	400	2.42	1.76
4	600	1.90	1.40

The computational cost of these FE models is very high due to severe deformation of matrix elements resulting in smaller time increments. The problem is catered by using mass scaling option available in ABAQUS/Explicit® [31]. The reduced characteristic distorted elements result in a

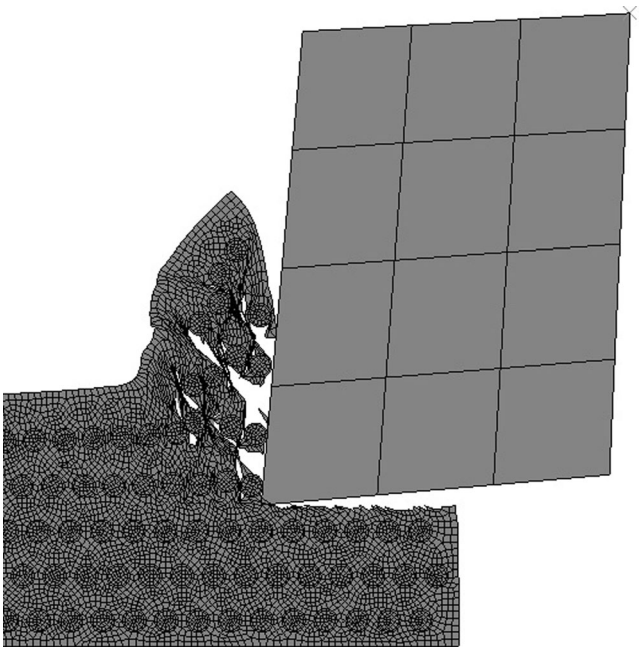

Fig. 3 Deformed mesh for model A

smaller global time increment. Scaling the mass of these elements as required throughout the simulation can significantly decrease the computation time. For cases in which the compressed elements are impacting a stationary rigid body, increases in mass for these small elements during the simulation will have very little effect on the overall dynamic response.

3 Results

The deformed meshes for the two models A and B are shown in Figs. 3 and 4. Both models are developed without cohesive elements. In model A, no parting line is used and a shear failure criterion is applied to the whole workpiece, whereas in model B, shear failure is only applied to the parting line. As the explicit dynamic simulations are highly sensitive to excessive mesh distortion, the use of parting line aligned the particles along the tool path in a horizontal fashion. This facilitates tool penetration and corresponding shear failure of the element before excessive distortion.

It has been observed that both the models are unable to simulate reinforcement debonding at the initial stages due to tool loading. However, debonding of reinforcement particles in model A occurred due to material failure around the reinforcement particles, and the model is able to simulate tool-particle interaction. In contrast, model B simulates a continuous chip with severe material deformation around the reinforcement particles. Experimental studies done by Fathipour et al. [32] showed serrated chips when machining the same workpiece material at similar conditions.

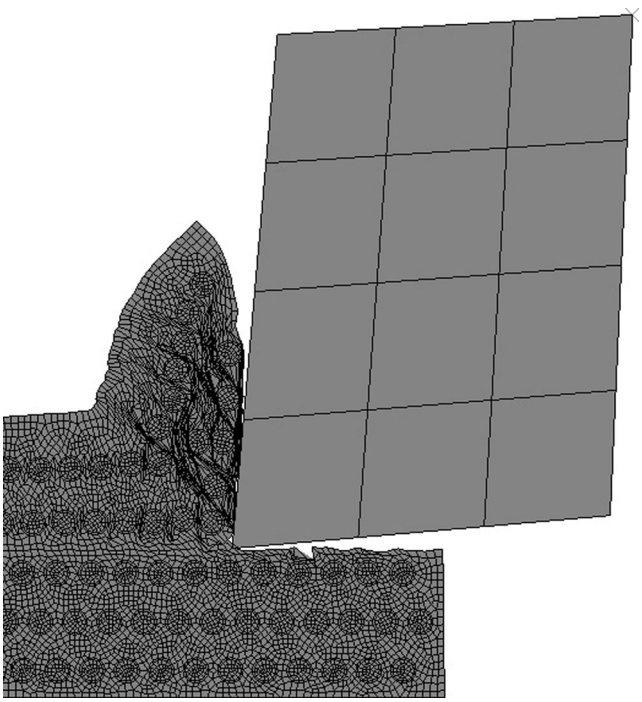

Fig. 4 Deformed mesh for model B

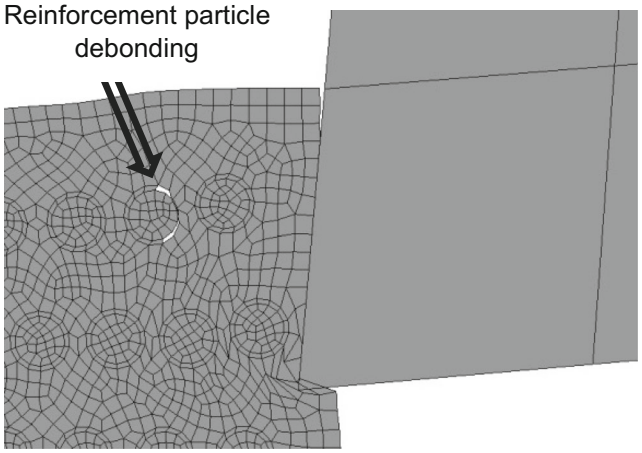

Fig. 5 Debonding initiates

Models C and D are developed using CZE around the reinforcement particles to simulate debonding at the interface. Shear failure is applied to the whole workpiece in both models; however, model D utilizes a parting line to minimize excessive mesh distortion. Also, elements are not being deleted in all shear failure models and retain some stiffness throughout the simulation time. Both models are successful in modeling the debonding of the reinforcement particles due to tool loading. Initial deformed meshes for model C are shown in Figs. 5 and 6, simulating the debonding of the reinforcement particle.

Cutting and thrust forces obtained from the experiments [22] and FE model are shown in Fig. 7. Both models A and B underestimate forces due to absences of cohesive forces around the reinforcement particles. Cutting forces are lowest for model A due to the application of shear failure model for

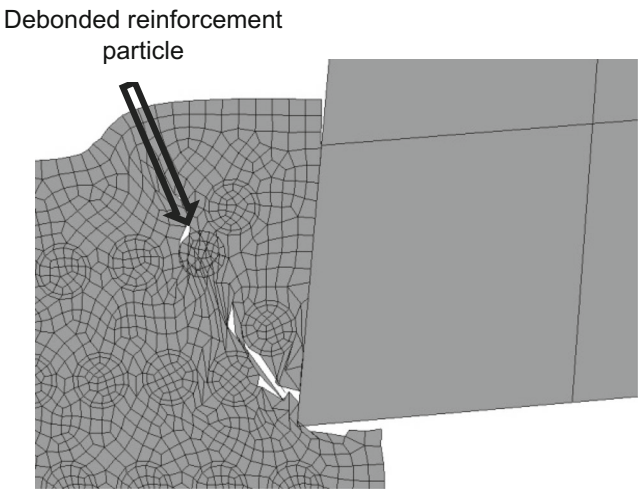

Fig. 6 Debonding completed

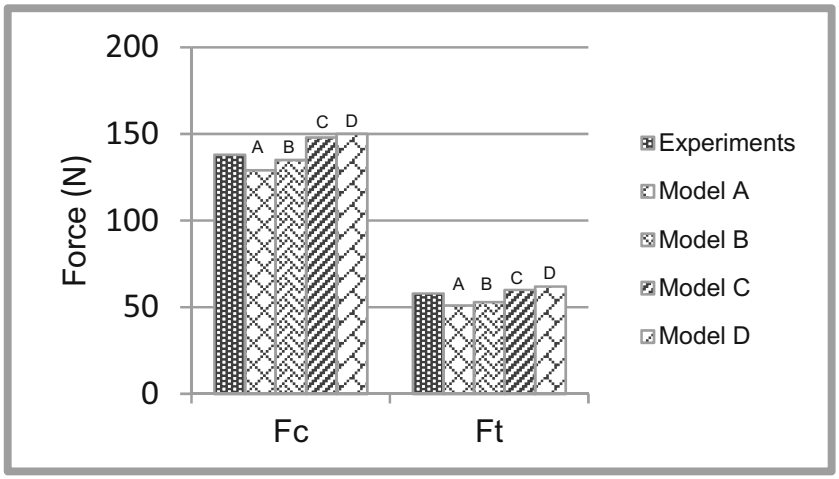

Fig. 7 Cutting and thrust forces

the whole workpiece in comparison to model B. Models C and D predict higher forces due to the use of cohesive elements and show minimal differences due to the use of parting line in front of the tool tip.

Mises stress for the FE models are shown in Figs. 8, 9, 10 and 11.

The stress distribution pattern for all the models appears to be very same. Due to the huge differences in the stress level for the reinforcement and matrix, the maximum stress is set to 700 MPa to better visualize the stress variation in the workpiece matrix. Mises stresses are lowest for model A due to shear failure and utilization of no cohesive elements. The chip morphology for all the four models can also be investigated by these figures. The waviness pattern on the back of chips can be seen for models with cohesive elements. This is the result of debonding of reinforcement particles and high matrix deformation due to the developing gaps. In model A, serration is mostly because of matrix element failure and there is no mechanism of debonding of reinforcement particles except complete material damage around the particle. In C and D, serration is due to gradual debonding of the reinforcement particles and hence it is comparatively less due to the presence of cohesive forces.

Model D performs better with regard to mesh distortion problem and shows a realistic deformed chip thickness. Also, shear localization can also be easily realized for model D. For model C, the matrix elements along the chip interface are failed and overlap with chip face. Hence, the cohesive models work better with a predefined parting line.

The element library in ABAQUS® [33] does not support temperature degree of freedom for cohesive elements. Hence, models C and D are unable to predict temperature distributions.

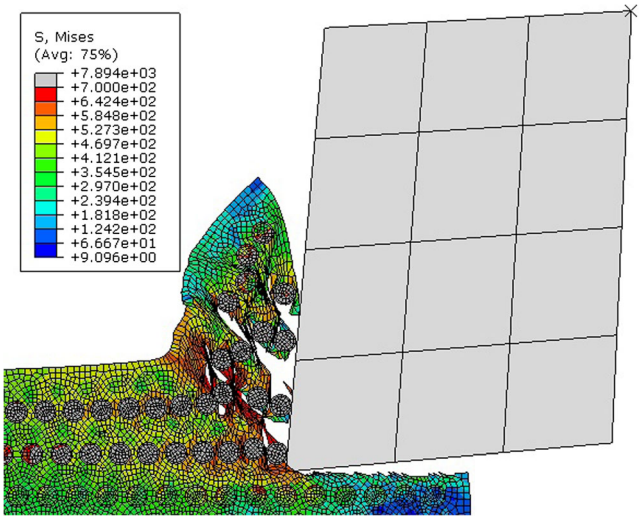

Fig. 8 Mises stress for model A

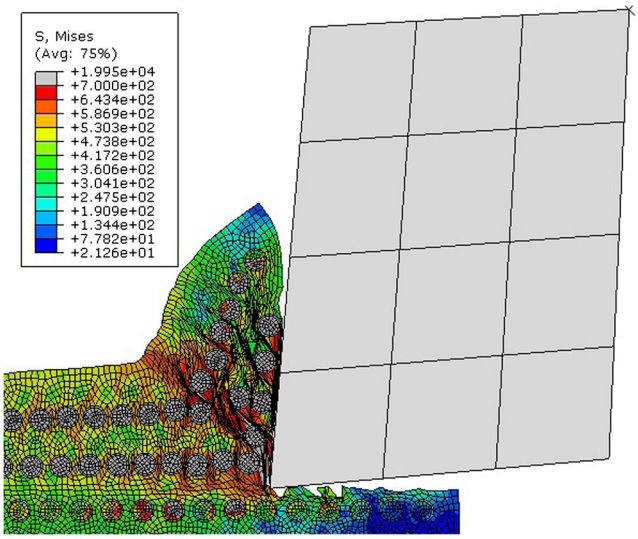

Fig. 9 Mises stress for model B

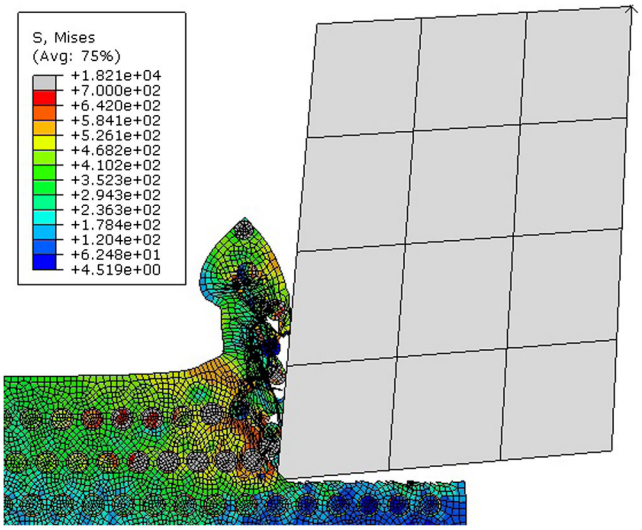

Fig. 10 Mises stress for model C

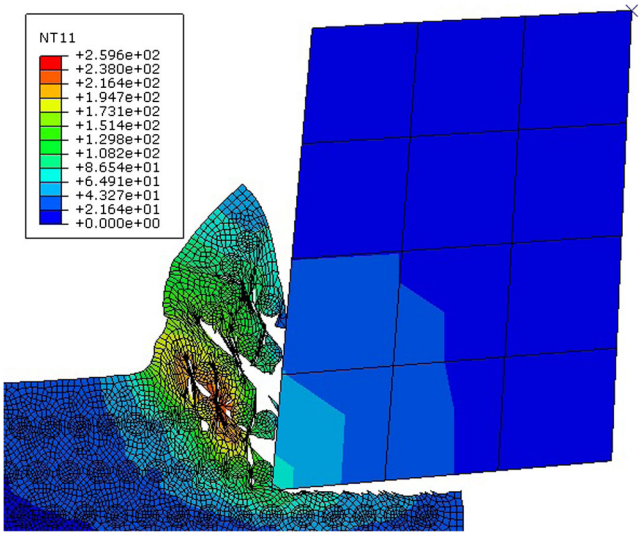

Fig. 12 Temperature contour for model A

Temperature distributions for models A and B are shown in Figs. 12 and 13. As expected, temperatures are lower for model A due to deletion of highly distorted elements. The range of temperatures predicted by model B is in close agreement with the results obtained by Zhu and Kishawy [3] while machining aluminum-based MMCs at similar cutting conditions. For both models, higher temperatures are predicted corresponding to the region of maximum deformation of the workpiece material around the hard reinforcement particles.

4 Conclusions

- The developed 2D FE models are successful in predicting the cutting performance variables like chip morphology, cutting forces, temperature, and stress distributions.
- Models with a cohesive element interface are able to simulate debonding of the reinforcement particles from the workpiece matrix.
- Models with cohesive elements show higher cutting forces as compared to noncohesive models.
- The range of temperatures predicted by FE models in agreement with the published results and high temperatures is confined to the region of maximum workpiece deformation.
- The FE model based on cohesive elements with a predefined parting line performs better to simulate serrated chips and shows shear localized regions around the chip face.

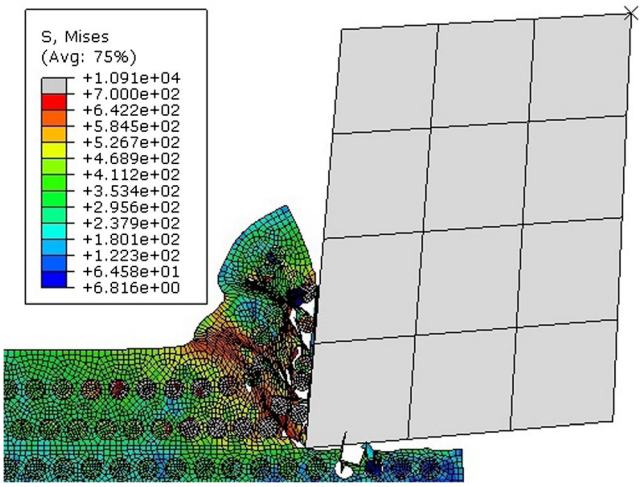

Fig. 11 Mises stress for model D

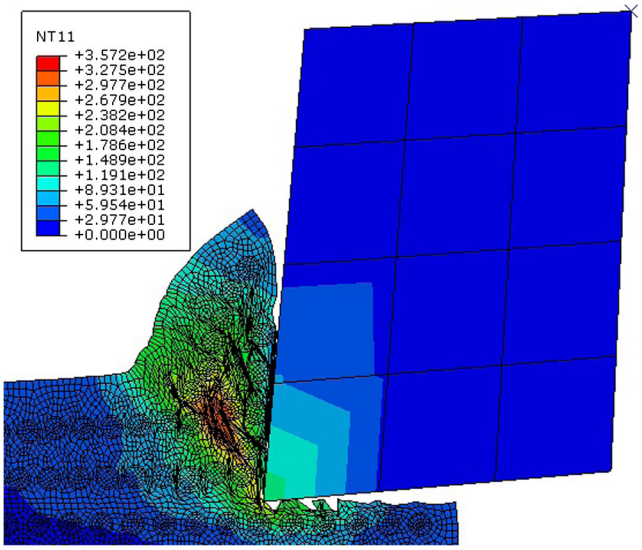

Fig. 13 Temperature contour for model B

Acknowledgments The project is financially supported by King Saud University, Vice Deanship of Research Chairs.

References

1. Chawla KK, Chawla N(2006) Metal-matrix composites. Wiley Online Library
2. Shin Y, Dandekar C (2012) Mechanics and modeling of chip formation in machining of MMC. Machining of metal matrix composites, J. P. Davim, ed., Springer London, pp. 1–49
3. Zhu Y, Kishawy HA (2005) Influence of alumina particles on the mechanics of machining metal matrix composites. Int J Mach Tools Manuf 45(4):389–398
4. Looney LA, Monaghan JM, O'Reilly P, Taplin DMR (1992) The turning of an Al/SiC metal-matrix composite. J Mater Process Technol 33(4):453–468
5. Schwartz MM (1997) Composite materials. Volume 2: Processing, fabrication, and applications
6. Muthukrishnan N, Murugan M, Rao KP (2008) An investigation on the machinability of Al-SiC metal matrix composites using PCD inserts. Int J Adv Manuf Technol 38(5–6):447–454
7. Weinert K, König W (1993) A consideration of tool wear mechanism when machining metal matrix composites (MMC). CIRP Ann Manuf Technol 42(1):95–98
8. Quigley O, Monaghan J, O'Reilly P (1994) Factors affecting the machinability of an Al/SiC metal-matrix composite. J Mater Process Technol 43(1):21–36
9. Manna A, Bhattacharayya B (2003) A study on machinability of Al/SiC-MMC. J Mater Process Technol 140(1):711–716
10. Manna A, Bhattacharyya B (2004) Investigation for optimal parametric combination for achieving better surface finish during turning of Al/SiC-MMC. Int J Adv Manuf Technol 23(9–10):658–665
11. Manna A, Bhattacharayya B (2005) Influence of machining parameters on the machinability of particulate reinforced Al/SiC–MMC. Int J Adv Manuf Technol 25(9–10):850–856
12. El-Gallab M, Sklad M (1998) Machining of Al/SiC particulate metal-matrix composites: part I: tool performance. J Mater Process Technol 83(1):151–158
13. Camus G (2000) Modelling of the mechanical behavior and damage processes of fibrous ceramic matrix composites: application to a 2-D SiC/SiC. Int J Solids Struct 37(6):919–942
14. Arola D, Ramulu M (1997) Orthogonal cutting of fiber-reinforced composites: a finite element analysis. Int J Mech Sci 39(5):597–613
15. Nayak D, Bhatnagar N, Mahajan P (2005) Machining studies of UD-FRP composites part 2: finite element analysis. Mach Sci Technol 9(4):503–528
16. Venu Gopala Rao G, Mahajan P, Bhatnagar N (2007) Machining of UD-GFRP composites chip formation mechanism. Compos Sci Technol 67(11):2271–2281
17. Monaghan J, Brazil D (1998) Modelling the flow processes of a particle reinforced metal matrix composite during machining. Compos A: Appl Sci Manuf 29(1):87–99
18. Ramesh MV, Chan KC, Lee WB, Cheung CF (2001) Finite-element analysis of diamond turning of aluminium matrix composites. Compos Sci Technol 61(10):1449–1456
19. El-Gallab MS, Sklad MP (2004) Machining of aluminum/silicon carbide particulate metal matrix composites: part IV. Residual stresses in the machined workpiece. J Mater Process Technol 152(1):23–34
20. Pramanik A, Zhang LC, Arsecularatne JA (2007) An FEM investigation into the behavior of metal matrix composites: tool–particle interaction during orthogonal cutting. Int J Mach Tools Manuf 47(10):1497–1506
21. Zhou L, Huang ST, Wang D, Yu XL (2011) Finite element and experimental studies of the cutting process of SiCp/Al composites with PCD tools. Int J Adv Manuf Technol 52(5–8):619–626
22. Dandekar CR, Shin YC (2009) Multi-step 3-D finite element modeling of subsurface damage in machining particulate reinforced metal matrix composites. Compos A: Appl Sci Manuf 40(8):1231–1239
23. Dandekar CR, Shin YC (2010) Laser-assisted machining of a fiber reinforced metal matrix composite. J Manuf Sci Eng 132(6):061004
24. Iordanoff I, Richard D, Tcherniaieff S (2008) Discrete element method, a tool to investigate contacts in material forming. Int J Mater Form 1(1):1235–1238
25. Iliescu D, Gehin D, Iordanoff I, Girot F, Gutiérrez ME (2010) A discrete element method for the simulation of CFRP cutting. Compos Sci Technol 70(1):73–80
26. Chen Y, Kulasegaram S (2009) Numerical modelling of fracture of particulate composites using SPH method. Comput Mater Sci 47(1):60–70
27. Medina DF, Chen JK (2000) Three-dimensional simulations of impact induced damage in composite structures using the parallelized SPH method. Compos A: Appl Sci Manuf 31(8):853–860
28. Madaj M, Píška M (2013) On the SPH orthogonal cutting simulation of A2024-T351 alloy. Procedia CIRP 8:151–156
29. Pantalé O, Bacaria JL, Dalverny O, Rakotomalala R, Caperaa S (2004) 2D and 3D numerical models of metal cutting with damage effects. Comput Methods Appl Mech Eng 193(39–41):4383–4399
30. Dandekar CR (2010) Multi-scale modeling and laser-assisted machining of metal matrix composites. Ph.D thesis, Purdue University
31. Mass scaling, analysis techniques, ABAQUS analysis user manual, ABAQUS Documentation V 6.10. Dassault Systems
32. Fathipour M, Zoghipour P, Tarighi J, Yousefi R (2012) Investigation of reinforced sic particles percentage on machining force of metal matrix composite. Modern Applied Science, 6(8)
33. Particle elements, ABAQUS analysis user manual, ABAQUS Documentation, V 6.10. Dassault Systemes